Effects of Chain Length on the Structure and Dynamics of Polyvinyl Chloride During Atomistic

**Molecular Dynamics Simulations** 

Feranmi V. Olowookere, Ali Al Alshaikh, Jason E. Bara, and C. Heath Turner\*

Department of Chemical and Biological Engineering, The University of Alabama, Tuscaloosa, AL

35487-0203, United States

**Abstract** 

Molecular dynamics (MD) simulations have proven to be useful for predicting and interpreting the conformational and dynamic properties of various polymer-solvent systems. The number of repeat units used to represent a polymer chain in an MD study is intended to provide a balance between the computational demands and the reliability of the specific phenomena being studied. To date, this balance has not received sufficient attention. Here, we investigate how the chain length of an atomistic polymer model influences the structure and dynamics of the polymer in different solvents. Seven different polyvinyl chloride (PVC) models, ranging from 5 to 240 –(CH<sub>2</sub>CHCl)- repeat units, are studied using atomistic MD simulations in two polar organic solvents: tetrahydrofuran (THF) and dimethylformamide (DMF). After benchmarking our MD results against experimental density data, we calculate polymer end-to-end distances, radii of gyration, radial distribution functions, shape descriptors, end-to-end vector correlation functions, dihedral autocorrelation functions, surface areas, surface electrostatic potentials, glass transition temperature and melt viscosities. Our MD simulations demonstrate that most of these properties converge when approximately 100-120 repeat units are used to represent PVC, and this convergence behavior is observed in different solvents and at different temperatures.

Keywords: Polymers; chain length; molecular dynamics; polyvinyl chloride

\*Corresponding author contact:

C. Heath Turner

E-mail address: <a href="https://https

Phone number: 205-348-1733

1

#### 1. Introduction

Given the urgent need to develop more environmentally-benign and efficient polymer recycling processes, it is imperative to gain more mechanistic insights into polymer-solvent interactions and to design sustainable solvent formulations through molecular design strategies [1]. Common theoretical techniques for studying interactions in polymer-solvent systems include models such as the Flory-Huggins (FH) [2], Debye-Huckel (DH) [3], Poisson-Boltzmann (PB) [4], and Hansen & Hildebrand solubility models (HH) [5]. The HH and FH models are mainly focused on predicting polymer solubility in solvents, while DH and PB theories describe electrostatic interactions in solution. The HH solubility models are based on solute-solvent interaction, whereas the FH theory assumes a random distribution of polymer and solvent molecules in solution. The PB theory is predominantly used for studying biomolecules, while the DH theory is more broadly applicable to ionic solutions. While these models can provide valuable guidance, their fundamental simplicity makes it difficult to capture many of the complexities encountered in polymer-solvent systems. In conjunction with these theoretical models, various experimental techniques have been used to quantify (or infer) the interactions within polymer-solvent systems, such as viscosity measurements, light scattering, X-ray scattering, and infrared (IR) spectroscopy [6-10].

Molecular dynamics (MD) simulations are a complementary tool for evaluating polymer-solvent interactions and for gaining insights into the molecular-level behavior of these polymer systems, including both structural and dynamic properties. MD simulations of polymer systems first emerged in the literature several decades ago [11, 12]. Most of the early work focused on very simple systems, such as alkane chains (or polymer chains composed of alkane monomers, such as polyethylene) and bead and spring models [13, 14]. Since then, simulation studies have been conducted to extensively examine more complex polymer-solvent systems across a wide range of polymer chain lengths [15]. For instance, Steinhauser [16] used a coarse-grained (CG) bead spring model of 50-400 repeat units to examine the

conformational behavior of long linear polymer chains by calculating the gyration tensors and form factors. Also, classical density functional theory (DFT) and MD simulation have been used to investigate dilute and semi-dilute solutions of polymer nanoparticle composites near a solid surface [17]. By testing N = 10 and N = 40 repeat units, it was concluded that longer chain lengths improve the surface coverage of the polymer segments. On the other hand, Harmandaris [18] used MD simulations to model polydisperse linear polyethylene (PE) melts (ranging from PE<sub>20</sub> to PE<sub>150</sub>). They calculated fundamental properties such as the radius of gyration ( $R_g$ ), end-to-end distance, radial distribution functions (RDFs), and end-to-end vector autocorrelation functions, considering the differences in properties of longer polymer chains. A minimal chain length value of approximately C<sub>60</sub> was identified, beyond which the chain length independent parameters can be considered a constant (i.e., the PE model starts behaving more like a polymer versus a long alkane). To the best of our knowledge, PE<sub>150</sub> is the longest synthetic polymer ever simulated with a fully atomistic model in MD [19].

Due to the increasing performance of modern computers, as well as advancements in algorithms, it is now possible to use MD simulations to model relatively large polymers using atomistic force fields. In conjunction, a variety of computational methods have recently been developed to help characterize the mechanical, physical, and chemical behavior of polymers in different applications [20-24], such as the polymer behavior underlying the fundamental mechanisms of molecular imprinting [21].

Among synthetic polymers, polyvinyl chloride (PVC) is one of the most common thermoplastics in use worldwide, with ~40 Mt produced annually [25]. However, recycling PVC via conventional (i.e. thermomechanical) methods is problematic, and thus, PVC has recently gained attention as a viable candidate for upcycling from a waste plastic to other value-added products [25-27]. MD simulations can potentially provide valuable insights to guide the design of new, environmentally benign solvents for processing PVC waste. However, from an MD modeling perspective, it is important to know the minimum

system size (e.g., PVC chain length) necessary to obtain converged material properties. Currently, this information is lacking with respect to many synthetic polymer models. For instance, very little guidance is available in the literature regarding the effects of the PVC chain length on its simulated structural or dynamic properties, and the few studies that exist have modeled polymers of arbitrary length [16-19, 28, 29]. Recent studies, particularly on PVC, have not directly explored or explained the impacts of selecting different polymer chain lengths on the predicted polymer properties. Some MD investigations indicate the need to minimize computational costs, and therefore, choose to model relatively short polymers. While others claim that longer polymer chains are needed to properly capture phenomena induced by entanglements. In the present work, we define different PVC chain lengths as PVC<sub>N</sub>, where N is the number of –(CH<sub>2</sub>CHCl)- repeat units. Two different atomistic PVC models (PVC<sub>76</sub> and PVC<sub>153</sub>) were investigated by Neelov et al. [28], while in another case, nanoparticles composed of PVC<sub>10</sub> were used by Li et al. [29] to simulate PVC interactions with a model membrane. Considering these previous studies, more information is needed about the reliability of using different PVC chain lengths in MD simulations.

The behavior of PVC has been previously experimentally studied in a variety of different solvents, including tetrahydrofuran (THF), N-methyl-2-pyrrolidone (NMP), and N,N-dimethylformamide (DMF) to determine the degree of polymer-solvent interaction [7]. The experimental studies are typically conducted with PVC molecular weights that are much higher ( $M_N \sim 200 \, \text{kg/mol}$ ) than what can be normally simulated in an atomistic MD simulation ( $\sim 5 \, \text{kg/mol}$ ). Thus, it is critical to understand the impact of PVC chain length on the simulated behavior to help design the most appropriate model system, i.e., a system that is large enough to minimize finite-size effects, yet one that is still computationally tractable.

To address this balance in model design, atomistic simulations have been either constrained to arbitrary chain lengths or CG models have been used to extend the time and length scales accessible [30-32]. For instance, CG models have been used to simulate systems with chains of up to 2000 beads long

 $(M_N = \sim 32 \text{ kg/mol})$  at time scales of up to  $10^{-6}$  to  $10^{-3}$  s. These CG models have also been used to explore the effects of (long) polymer chain lengths on the aggregation and dispersion of nanoparticles in polymer melts [33]. However, it can be challenging to capture site-specific interactions with CG models, and dynamic properties are often highly skewed when using CG models.

This work aims to identify the tradeoff in the structural and dynamic properties of a solvated polymer model (specifically PVC), as a function of the chain length when performing atomistic MD simulations. Seven different PVC models are simulated in two different solvents, with polymer chain lengths ranging from PVC<sub>5</sub> to PVC<sub>240</sub>; several experimental benchmarks are included to help evaluate the reliability of the model predictions. Overall, we find that most of the polymer properties investigated converge when model sizes of PVC<sub>120</sub> or larger are used.

## 2. Methodology

The MD simulations were performed using the Gromacs 2021.1 simulation package [34, 35], and VMD [36] was used for visualization purposes. Seven different PVC models (Figure 1) of varying chain lengths were investigated in both THF and DMF, and the OPLS-AA force field [37] was used to describe the bonded and non-bonded interactions (Figure 1). PolyParGen with the *ab-initio* HF STO-3G method [38] was used to obtain the OPLS-AA parameters and atomic charges within the polymer, respectively, while LigParGen with the 1.14\*CM1A-LBCC method [39, 40] was used to obtain the OPLS-AA parameters and atomic charges of the solvents, respectively. The PACKMOL package [41] was used to obtain the initial configurations of the solvent and PVC molecules. In this work, we simulated systems containing ~10 wt./wt.% PVC in solvent, similar to the compositions of the corresponding experiments. The number of molecules in each system is shown in Table 1. Five independent replicas of each system are simulated to generate statistical confidence integrals for the computed properties.

The initial system configurations were first minimized by employing the steepest descent method. Then, an annealing process was implemented, whereby each system was subjected to high temperature (T = 800 K) in the NVT ensemble and then cooled to T = 323 K in 25 ns. The system was then subjected to high pressure (P = 100 bar) in the NPT ensemble before being reduced to P = 1 bar in 25 ns. Following that, the NPT ensemble went through an equilibration stage for 50 ns, in which the velocity rescaling thermostat [42] and the Parrinello-Rahman barostat [43] were used to keep the pressure and temperature constant (with time constants of 5 ps and 0.1 ps, respectively). After these equilibration stages, the relevant properties were computed during a 50 ns production run, with results collected every 30 ps. The statistical uncertainties were obtained via a block-averaging method with 5 ns sub blocks. In accordance with the force field used, the Lennard-Jones potential was used to represent van der Waals interactions, with a 1.0 nm cut-off radius and geometric combination rules for unlike pair interactions. Long-range electrostatic interactions beyond a cut-off radius of 1.0 nm were also calculated using the Particle Mesh Ewald (PME) method [44]. The LINCS algorithm [45] was used to constrain the hydrogen bond lengths, and periodic boundary conditions were imposed in all three dimensions.

The Gromacs package utilities gmx rdf, gmx distance, gmx gyrate and gmx angle were used to determine the RDFs, end-to-end distances,  $R_g$ , and dihedral autocorrelation functions, respectively. The end-to-end autocorrelation functions were calculated using the reorientation dynamics tool in the TRAVIS package [46], while the surface area and electrostatic potential were obtained using an in-house code.

**Table 1.** Composition details of each system simulated.

	Molecular weight of PVC (g/mol)	No. of solvent molecules (THF, DMF)	Wt. % PVC (THF)	Wt. % PVC (DMF)
PVC <sub>5</sub>	313.5	40	9.80	9.68
$PVC_{20}$	1,251	156	10.01	9.89
$PVC_{40}$	2,501	312	10.01	9.88
PVC <sub>60</sub>	3,751	470	9.97	9.84

$PVC_{100}$	6,251	783	9.97	9.85
$PVC_{120}$	7,501	940	9.96	9.84
$PVC_{240}$	15,001	1,880	9.96	9.84

Fundamental size and shape properties of our polymer-in-solvent systems are calculated here to provide statistical descriptions of our polymer structures. For instance,  $R_g$  is used to estimate the magnitude of the random coil shape:

$$\langle R_g^2 \rangle = \frac{1}{2N^2} \sum_{n,m} \langle (r_n - r_m)^2 \rangle \tag{1}$$

where the coordinates of the n repeat units (n = 1...N) along the polymer chain are denoted by  $r_n$ , and the center-of-mass of the polymer is represented by  $r_m$ . Also, the principal moments of  $R_g$  ( $\lambda_x$ ,  $\lambda_y$ ,  $\lambda_z$ ) can be combined to generate several different shape parameters that describe the average structure of the polymer particles. These parameters include the asphericity (b), acylindricity (c), and anisotropy (k), and these terms are defined as:

$$b = \frac{3}{2}\lambda_z^2 - \frac{R_g^2}{2} \tag{2}$$

$$c = \lambda_y^2 - \lambda_z^2 \tag{3}$$

$$k = \frac{3}{2} \frac{\lambda_x^4 + \lambda_y^4 + \lambda_z^4}{(\lambda_x^2 + \lambda_y^2 + \lambda_z^2)^2} - \frac{1}{2}$$
 (4)

The end-to-end distance (R) of a polymer chain is calculated as the distance  $(r_i)$  between the carbon sites of the head and tail of the polymer, and it provides a good statistical measure of the polymer length:

$$\langle R \rangle = \sum_{i=1}^{n} r_i \tag{5}$$

Furthermore, the end-to-end vector reorientation dynamics of the polymers are analyzed in order quantify the system's dynamical heterogeneity. A Legendre polynomial  $P_n$  is applied to the dot product of the two vectors in TRAVIS, as shown in the correlation function  $C_n(\tau)$  below:

$$C_n(\tau) = \int_0^\infty P_n \left( \frac{u(t) \cdot u(t+\tau)}{\|u(t)\| \|u(t+\tau)\|} \right) dt \tag{6}$$

$$T_n = \int_0^\infty C_n(\tau) d\tau \tag{7}$$

The reorientation time  $T_n$  is thus an integral of the correlation function based on the system's trajectory. Because  $C_n(\tau)$  does not decay to zero, the integration cannot be performed directly. As a result, the function is fitted with a Levenberg-Marquardt minimizer [47], which is then analytically integrated to yield the reorientation time.

The dihedral autocorrelation function (DACF) is another dynamical tool for quantifying the temporal evolution and correlation of dihedral angles in a molecular system over time. The correlation function C(t) is defined as follows:

$$C(t) = \langle \cos(\theta(\tau) - \theta(\tau + t)) \rangle_{\tau}$$
(8)

where  $\theta$  is the dihedral angle between four consecutive carbon atoms of the polymer backbone, and  $\tau$  is the correlation time. It can also be rewritten as the sum of two products:

$$C(t) = \left\langle \cos(\theta(\tau)) \cos(\theta(\tau+t)) + \sin(\theta(\tau)) \sin(\theta(\tau+t)) \right\rangle_{\tau} \tag{9}$$

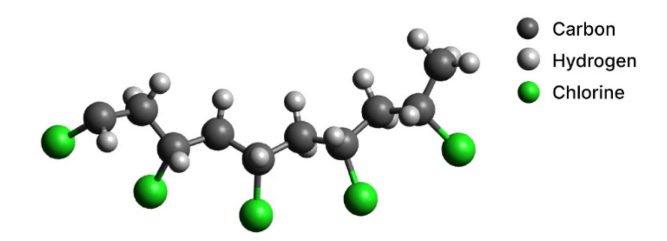
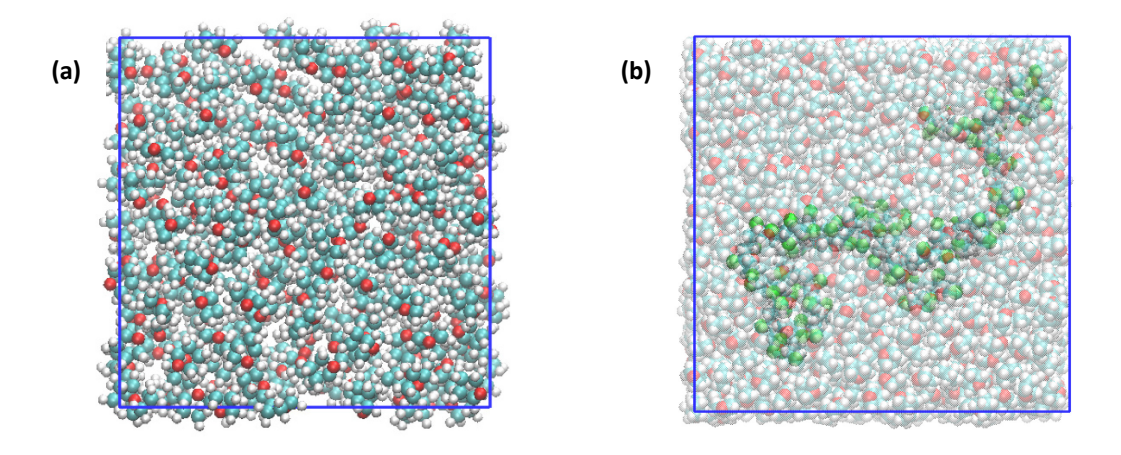


Figure 1. Molecular structure of PVC<sub>5</sub>.



**Figure 2.** Snapshots of the PVC-THF system; (a) THF molecules (b) PVC (bold) in THF (transparent); Color code: cyan = carbon, white = hydrogen, red = oxygen, green = chlorine

For an understanding of the mechanical and rheological properties of PVC, we also simulated separate melt systems (ranging from PVC<sub>5</sub> to PVC<sub>240</sub>), each comprising 50 chains. Specifically, the melt systems were annealed over 7 heating-cooling cycles, with the temperature being raised to 600 K and then lowered to 323 K for a total of 70 ns. The system was then equilibrated for 100 ns at 600 K and 1 bar, after which the relevant properties were computed during a 50 ns production run with results collected every 30 ps. To identify the glass transition temperature ( $T_g$ ), the systems were cooled to 100 K at a rate of 4 x 10<sup>-3</sup> K/ps. The systems were allowed to equilibrate at 5 ns intervals after every 20 K reduction. To obtain the  $T_g$  values, the volume was related to the temperature via a regularization function [48] described by Eq. 10:

$$V(T) = aT + b - c(T - T_g) \left[ 1 + \frac{(T - T_g)}{\sqrt{(T - T_g)^2 + \xi^2}} \right]$$
 (10)

where  $T_g$ , determined by non-linear regression, corresponds to the glass transition temperature, and  $\xi$  is the regularization parameter, where  $1 > \xi >>> 0$ . The parameters a, b, and c are obtained from the fitting of the data to the regularization function.

Shear viscosity ( $\eta$ ) was determined using non-equilibrium molecular dynamics simulations (NEMD) by employing the periodic perturbation technique [49]. This approach involves applying a periodic acceleration profile to the system as per Eq. 11, simulating the system's interaction with an external field:

$$a_{\chi}(z) = A\cos\left(\frac{2\pi z}{L_{\chi}}\right) \tag{11}$$

where A is the amplitude of the periodic profile and  $a_x$  is the x-component of the acceleration vector. When Newtonian fluids in steady-state under the Navier-Stokes equation are subjected to an external field of this nature, it results in a velocity profile shown in Eq. 12:

$$v_{\chi}(z) = V\cos\left(\frac{2\pi z}{L_z}\right) \tag{12}$$

where the amplitude V is proportional to the inverse of the viscosity following:

$$V = \frac{A\rho}{\eta} \left(\frac{L_z}{2\pi}\right)^2 \tag{13}$$

We conducted five 2 ns NEMD simulations, each with varying A values of 0.1, 0.075, 0.05, 0.01, and 0.0025 nm ps<sup>-2</sup>. Steady state was achieved within 1 ns, so we utilized the final 1 ns to derive the average of V. Considering the importance of sampling frequency in viscosity calculation, the data was

gathered every picosecond for these simulations. This facilitated the extrapolation of  $\eta$  towards zero perturbation.

#### 3. Results

## 3.1 System Densities

Tables 2 and 3 summarize the average simulated densities of the polymer solutions in this work, as well as a relative comparison of the densities to the longest polymer model, PVC<sub>240</sub>. By default, all simulated data correspond to T = 323 K, unless otherwise specified. As the chain lengths are increased, the system density values converge to ~878 kg/m³ in THF and ~971 kg/m³ in DMF, and the values agree very well with the experimental data. As a comparison, simulations were also performed at T = 298 K and 400 K (see Supporting Information), and similar convergence trends are found. To adequately sample the configuration space, the equilibration times were extended to 200 ns for PVC<sub>100</sub>, PVC<sub>120</sub>, and PVC<sub>240</sub> chains. Moreover, the simulation boxes were enlarged for the longer chains to prevent PVC-PVC mirror interactions.

**Table 2.** Average bulk density, end-to-end distance, and radius of gyration of PVC in the THF solvent. The density deviation is calculated with respect to the PVC<sub>240</sub> system. The density in parenthesis corresponds to the experimental value, with an error of 5% (MW  $\sim 48,000$ ).

No. of PVC	Density	% Density	R (nm)	$R_g$ (nm)
repeat units	$(kg/m^3)$	deviation		
5	871.1	-0.76	$1.26 \pm 0.28$	$0.38 \pm 0.02$
20	883.0	+0.59	$1.67 \pm 0.33$	$0.89 \pm 0.12$
40	889.6	+1.34	$1.76 \pm 0.48$	$1.46 \pm 0.25$
60	882.3	+0.51	$2.04 \pm 0.52$	$1.91 \pm 0.29$
100	875.1	-0.31	$2.36 \pm 0.64$	$1.98 \pm 0.27$
120	877.7	-0.01	$2.61 \pm 0.63$	$2.57 \pm 0.34$
240	877.8 (916.8)	0.00	$3.11 \pm 0.51$	$2.75 \pm 0.40$

**Table 3.** Average bulk density, end-to-end distance, and radius of gyration of PVC in the DMF solvent. The density deviation is calculated with respect to the PVC<sub>240</sub> system. The density in parenthesis corresponds to the experimental value, with an error of 5% (MW  $\sim 48,000$ ).

No. of PVC repeat units	Density (kg/m³)	% Density deviation	R (nm)	$R_g$ (nm)
5	974.4	+0.37	$0.90 \pm 0.10$	$0.38 \pm 0.02$
20	978.1	+0.75	$1.43 \pm 0.34$	$0.90 \pm 0.13$
40	980.0	+0.95	$1.70 \pm 0.52$	$1.36 \pm 0.19$
60	975.1	+0.44	$1.86 \pm 0.53$	$1.65 \pm 0.24$
100	985.1	+1.47	$2.55 \pm 0.55$	$2.13 \pm 0.23$
120	976.7	+0.61	$2.57 \pm 0.59$	$2.41 \pm 0.27$
240	970.8 (971.5)	0.00	$3.03 \pm 0.64$	$2.50 \pm 0.27$

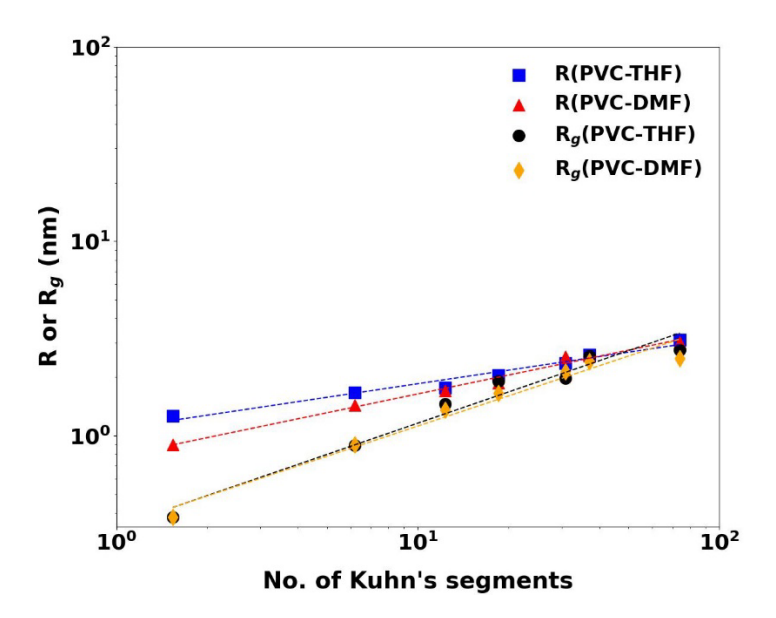
### 3.2 Radius of Gyration and End-to-End Distance

Tables 2 and 3 show the R and  $R_g$  values of the polymer chains in THF and DMF as a function of chain length. These values are commonly used to quantify the tendency to form the random coil structure that many polymers adopt in solution or in the amorphous bulk state. The  $R_g$  values increase in proportion to the length of the chain, and the R values of the chains exhibit a similar pattern. When plotted against the number of Kuhn's segments (which is the contour length divided by the Kuhn length), as shown in Figure 3, the R and  $R_g$  values exhibit a linear trend, similar to the results by Harmandaris [18]. The relationship between end-to-end distance and chain length satisfies the power law relationship in random walk and self-avoiding random walk,

$$R \sim bN^{\nu} \tag{14}$$

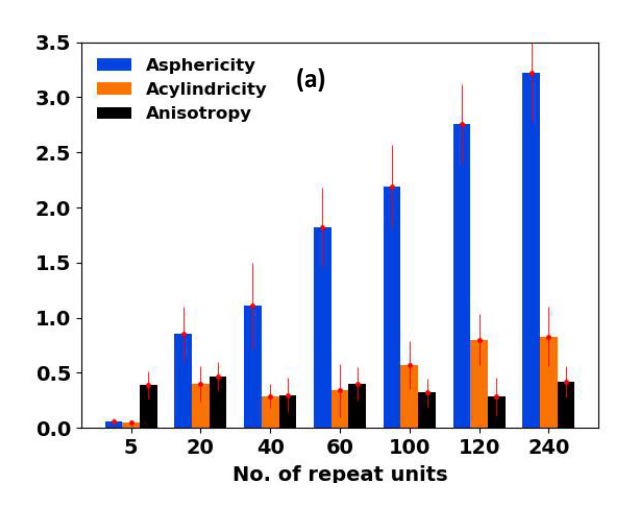
where b is the monomer-monomer distance (center of mass); v is the size exponent, where v = 1/2 for random walk and v = 3/5 for self-avoiding random walk given by Flory theory [50]. For large enough

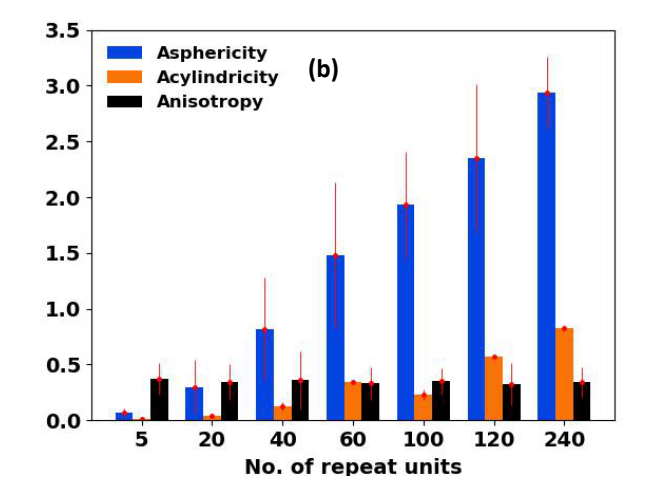
molecules with N >> 1, the radius of gyration is related to the mean end to end distance by  $R_g = \sqrt{\frac{3}{5}} R$ . In our current system, we obtain v = 0.48 ( $r^2 = 1.000$ ), with b = 0.248 nm and  $\frac{R_g}{R} = \frac{3}{4}$ .



**Figure 3.** End-to-end distance and radius of gyration (in nm) as a function of number of Kuhn's segments in THF and DMF solvents.

The shape descriptors (asphericity, acylindricity, and anisotropy) are obtained and presented in Figure 4 to further elucidate the polymer shape. These values, as defined in Eq. (2-4), measure the configurations with respect to the principal axis system. The asphericity parameter is smaller for short chain lengths because the conformations are almost spherically symmetric, but it dramatically increases for longer chains. The acylindricity values do not change as much as the asphericity values, but they do increase when the error bars are considered. The particle distribution is also cylindrically symmetric with respect to the two coordinate axes for shorter chain lengths. The relative shape anisotropy reveals further details. Increasing the chain length has no effect on this parameter, so the particle distribution is uniform in all directions; the values are all close to zero.

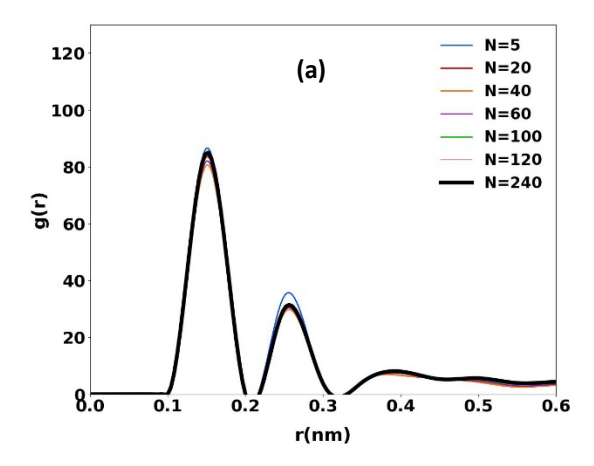


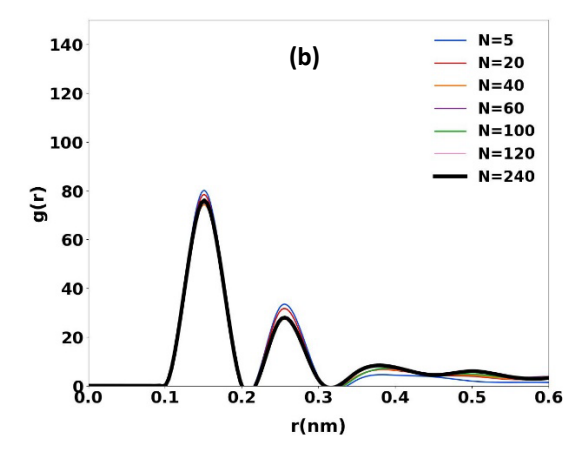


**Figure 4.** Shape descriptors (asphericity, acylindricity and anisotropy) of different chain lengths in (a) THF, (b) DMF; *note*: x-axis scale is not linear.

#### 3.3 Radial Distribution Function

Figure 5 shows the calculated intramolecular RDF for C-C atoms along the PVC backbone. As expected, the first peak occurs at 0.15 nm, which is the approximate C-C bond length. Both peaks at 0.15 nm and 0.25 nm are attributed to intramolecular correlations [51] due to the underlying polymer topology. The high peak intensities indicate that the C atoms in the respective systems are highly ordered.

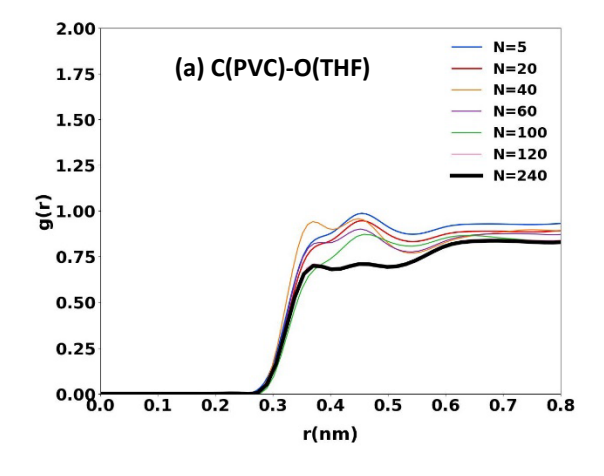


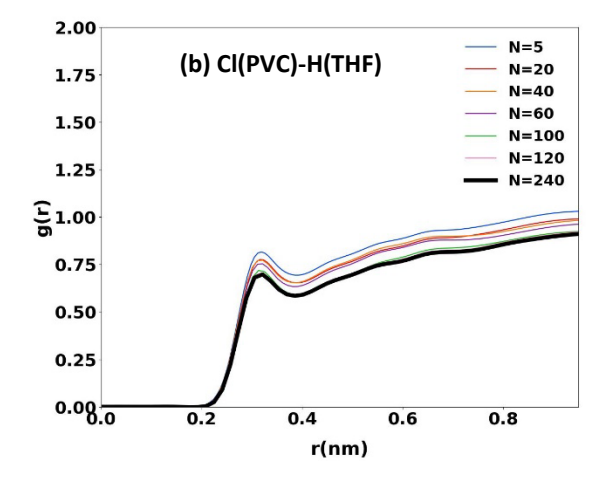


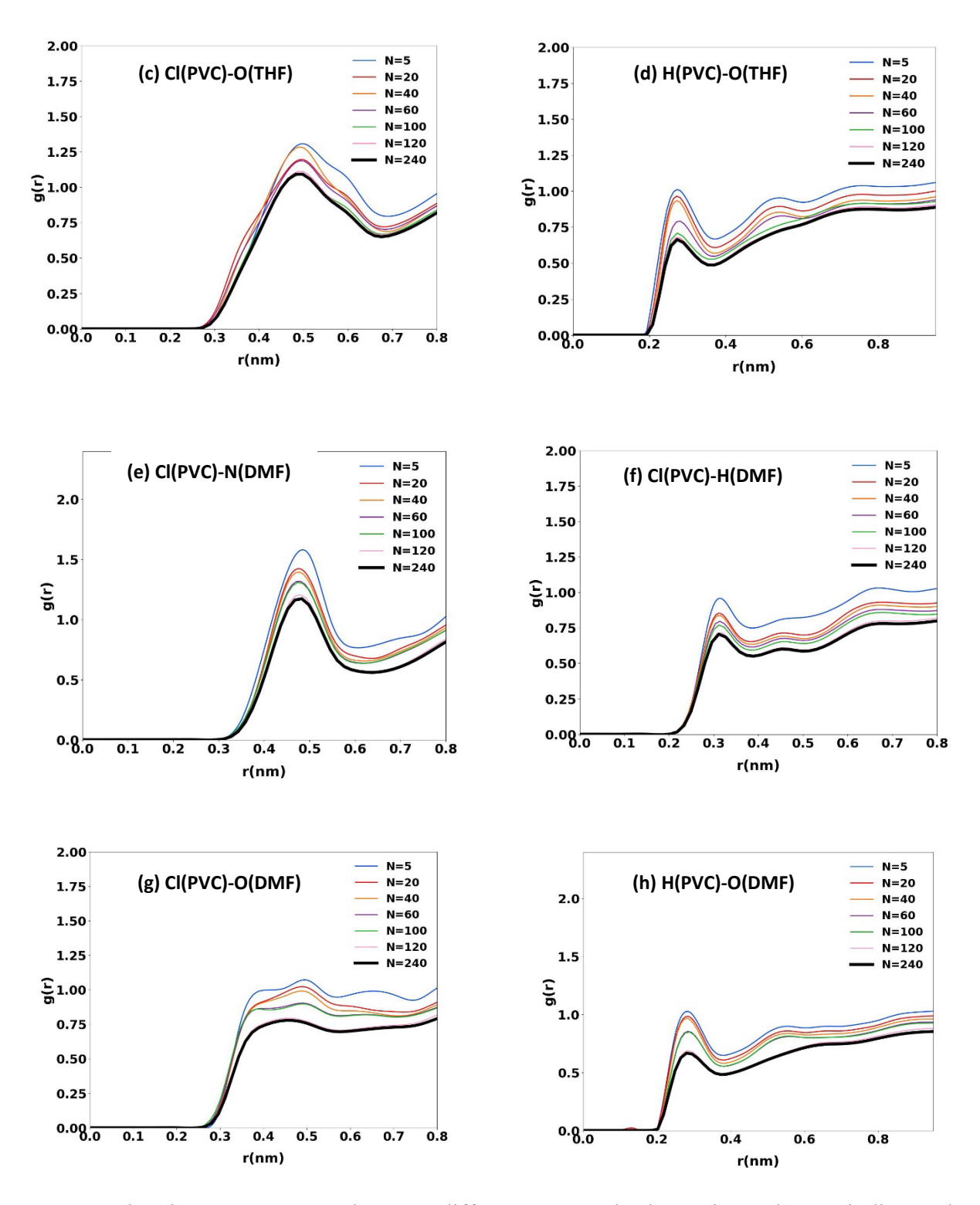
**Figure 5.** Intramolecular radial distribution function (RDF) of carbon-carbon (C-C) sites along the PVC backbone in (a) THF (b) DMF, where N indicates the number of repeat units.

The site-site radial distribution functions (RDFs) in Figure 6 show the presence of short-range interactions between the PVC and the solvent atoms in the system. The presence of the initial peaks at 0.3 nm (in Figures 6b and 6d) indicates that there is a primary interaction between the Cl and H atoms in PVC and the H and O atoms in THF, respectively. There is a secondary, weaker coordination between the C atoms of PVC and the O atoms of THF at a distance of around 0.55 nm (in Figures 6a). Similar trends are also observed in the RDF plots involving DMF.

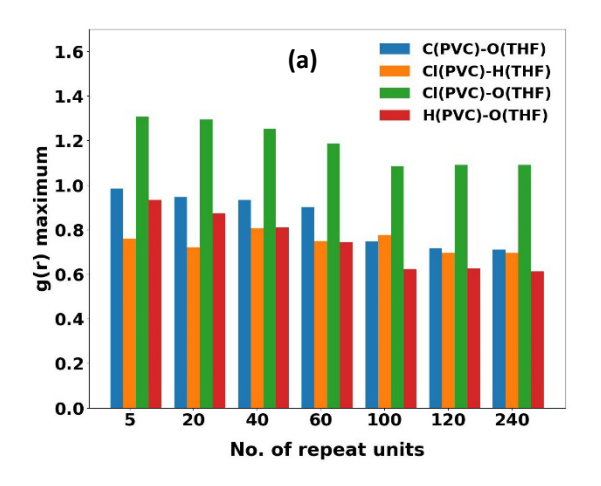
To further quantify the structural features of these systems, Figure 7 presents the magnitudes of the first peaks, as a function of increasing PVC chain length. The peak intensity is shown to decrease as the number of repeat units increases. The polymer structure tends to become less ordered with increasing chain length, and the peak intensities tend to converge at  $N = 100\sim120$ . Beyond just the magnitudes of the first peaks in the RDFs, the other features of the RDFs tend to adopt consistent characteristic patterns with PVC<sub>120</sub> models and longer.







**Figure 6.** Site-site RDFs at 323 K between different PVC and solvent sites, where N indicates the number of repeat units.



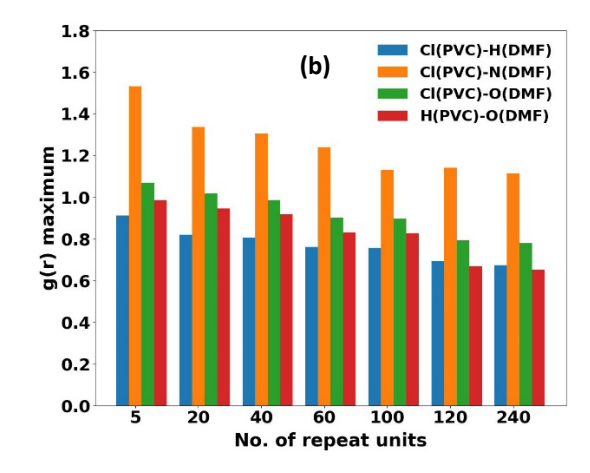


**Figure 7.** First peak intensity of (a) PVC-THF and (b) PVC-DMF RDFs as a function of the number of repeat units.

## 3.4 End-to-End Reorientation Dynamics

The structural characterization of the polymers in these solvents can be further quantified by evaluating the polymer dynamics via analyses of the end-to-end vector correlations of the PVC chains. The rate of correlation decay can be used to describe the orientation and translational dynamics of the end-to-end vectors of the polymer chains, as well as to infer the extent of chain stretching or contraction. Likewise, the value of the fitted time constant ( $\tau$ ) of the decay can be compared to the duration of the simulation to ensure that the maximum simulation time significantly exceeds the characteristic reorientation time. Figure 8 shows the time-dependent reorientation of the polymer end-to-end vectors for different PVC chain lengths. The time constant of the exponentially decaying autocorrelation function for PVC<sub>240</sub> is nearly 200 times smaller than that for PVC<sub>5</sub> in THF, indicating that the reorientation rate of the end-to-end vectors of the polymer chain is greatly influenced by chain length. Longer chains have a shorter reorientation time, implying that end-to-end vectors are less correlated. This behavior is also consistent with the end-to-end distance and  $R_g$ , which indicates that longer chains are more flexible. Similar trends are seen in DMF, but it appears that the end-to-end vectors of shorter chains appear to be

less correlated in DMF than THF. Figure 8c shows that the reorientation time decreases to  $\sim 0.1$  ns at N = 120 and above.

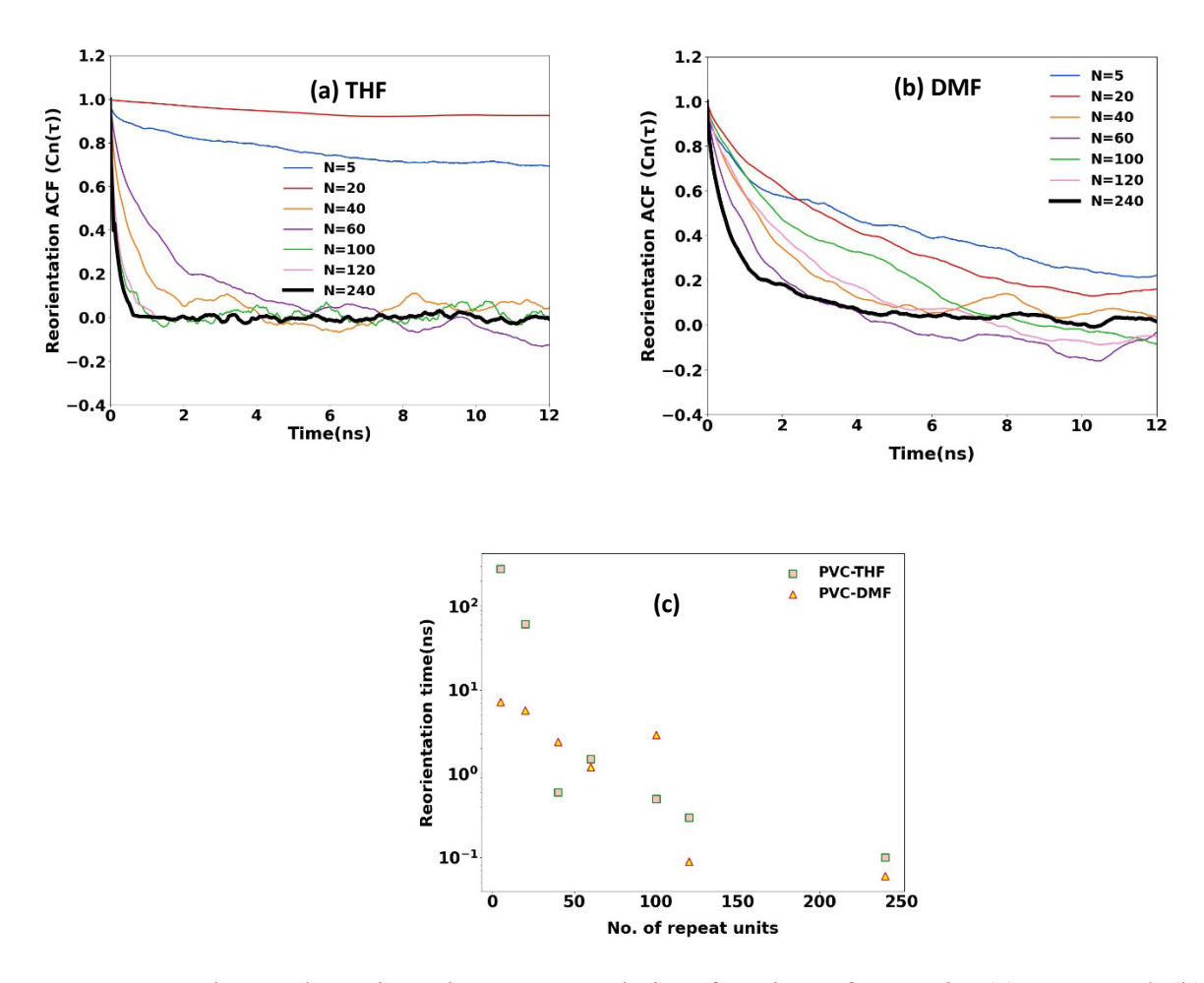


**Figure 8.** End-to-end reorientation autocorrelation function of PVC in (a) THF and (b) DMF; (c) reorientation time as a function of the number of repeat units.

### 3.5 Dihedral Autocorrelation Function

To understand the internal motion of the polymer chain, the decay of the dihedral angles along the PVC backbone is analyzed using the dihedral autocorrelation function (DACF), as shown in Eq. 8, to further describe the effects of chain lengths on the polymer dynamics. According to Figure 9, the DACF of shorter chains decays faster than that of the longer chains in both solvents, indicating that the dihedral angles in the shorter polymers rapidly decorrelates. The longer chain lengths tend to retard the dihedral

relaxation, likely due to entanglement and other intramolecular interactions; as the chain lengths increase, there are increased opportunities for repeat units to interact with themselves, creating energetic and steric barriers for dihedral motions. At polymer chain lengths of N = 100 and 120, the DACFs are very similar in shape and quantitatively very close to the longest polymer,  $PVC_{240}$ .

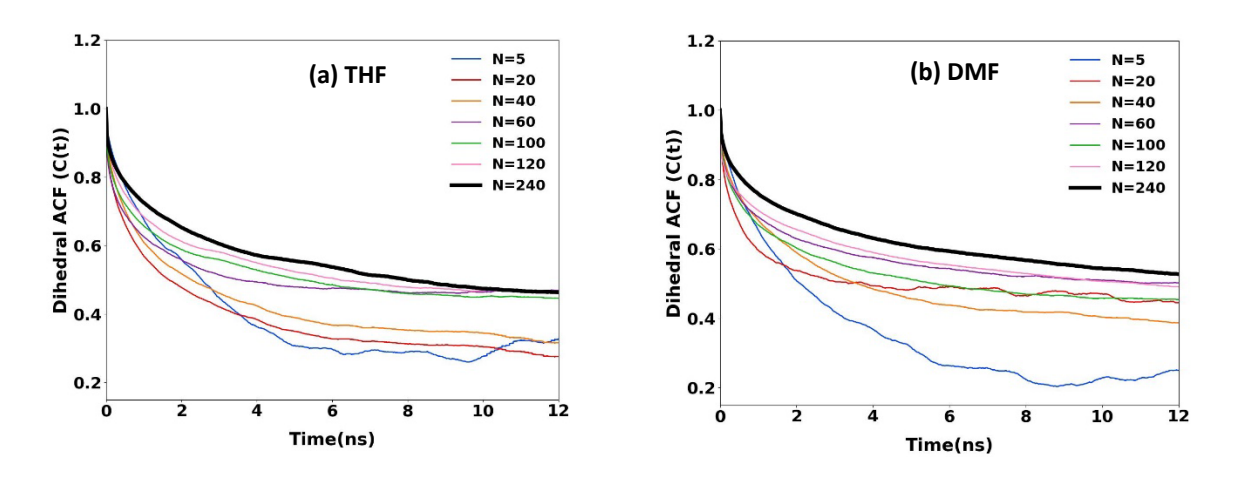


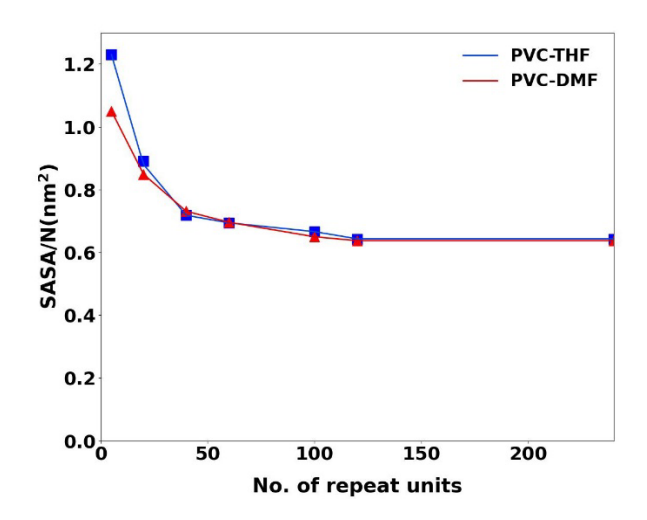
Figure 9. DACF of PVC in (a) THF and (b) DMF as a function of the number of repeat units.

#### 3.6 Solvent Accessible Surface Area and Electrostatic Potential

As shown in Figure 10, the normalized solvent accessible surface area (SASA/N) is plotted relative to polymer chain length. The SASA is defined as the surface created by the path traced by the center of a spherical probe, as it rolls along the van der Waals surface of the atoms (defined as the Lennard-Jones diameters of the atoms, taken from the OPLS-AA force field). Accordingly, as the SASA increases, more of the polymer is in contact with the surrounding solvent. In both THF and DMF, the surface area of PVC increases linearly with increasing chain length. When combined with the  $R_g$  value, the SASA is also an excellent indicator of changes in the polymer structure. Small chain lengths usually have lower theoretical surface area than the larger chains, which is supported by the low  $R_g$  values in Tables 2 and 3. When normalized by N, as shown in Figure 10, the surface area per repeat unit (SASA/N) is shown to deviate significantly among the shorter chains, but it eventually converges at N = 120 and above, reaching a

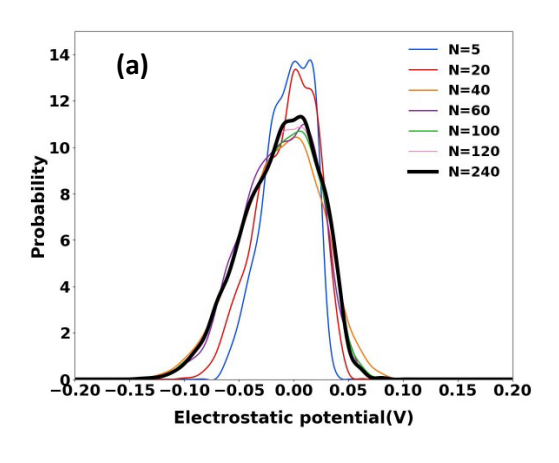
constant value of  $\sim$  0.64. Thus, beyond a minimal chain length (N  $\sim$  120), the surface area per repeat unit could potentially be used to estimate the SASA for much longer chains.

This convergence likely results from the interplay between entropy, which encourages a larger surface area per unit due to its preference for various configurations, and enthalpy, which reduces it to minimize potential energy. At N = 120, these contributions balance, leading to a stable polymer chain configuration.



**Figure 10.** SASA/N versus number of repeat units for PVC in THF and DMF solvents (using a probe diameter of 0.3 nm).

There is also a relationship between polymer chain length and the electrostatic potential (ESP) of the polymer SASA, as shown in Figure 11. At relatively short chain lengths ( $N = 5\sim20$ ), there can be significant deviations in the ESP distributions. These deviations could potentially lead to anomalous solvation behavior in different environments, especially depending on the polarity of the surrounding solvent. While there are still some small variations in the ESP among the different PVC models, the results tend to converge when using PVC<sub>40</sub> models and longer.



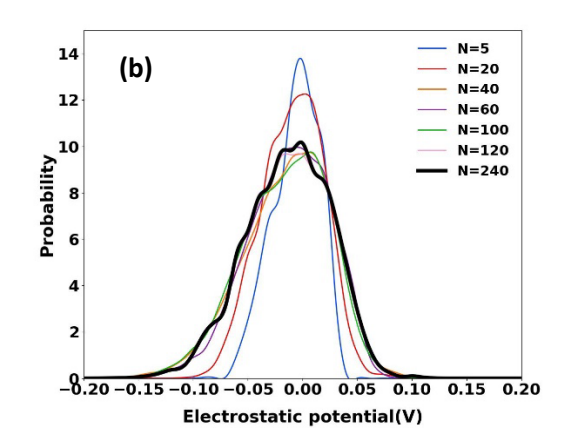
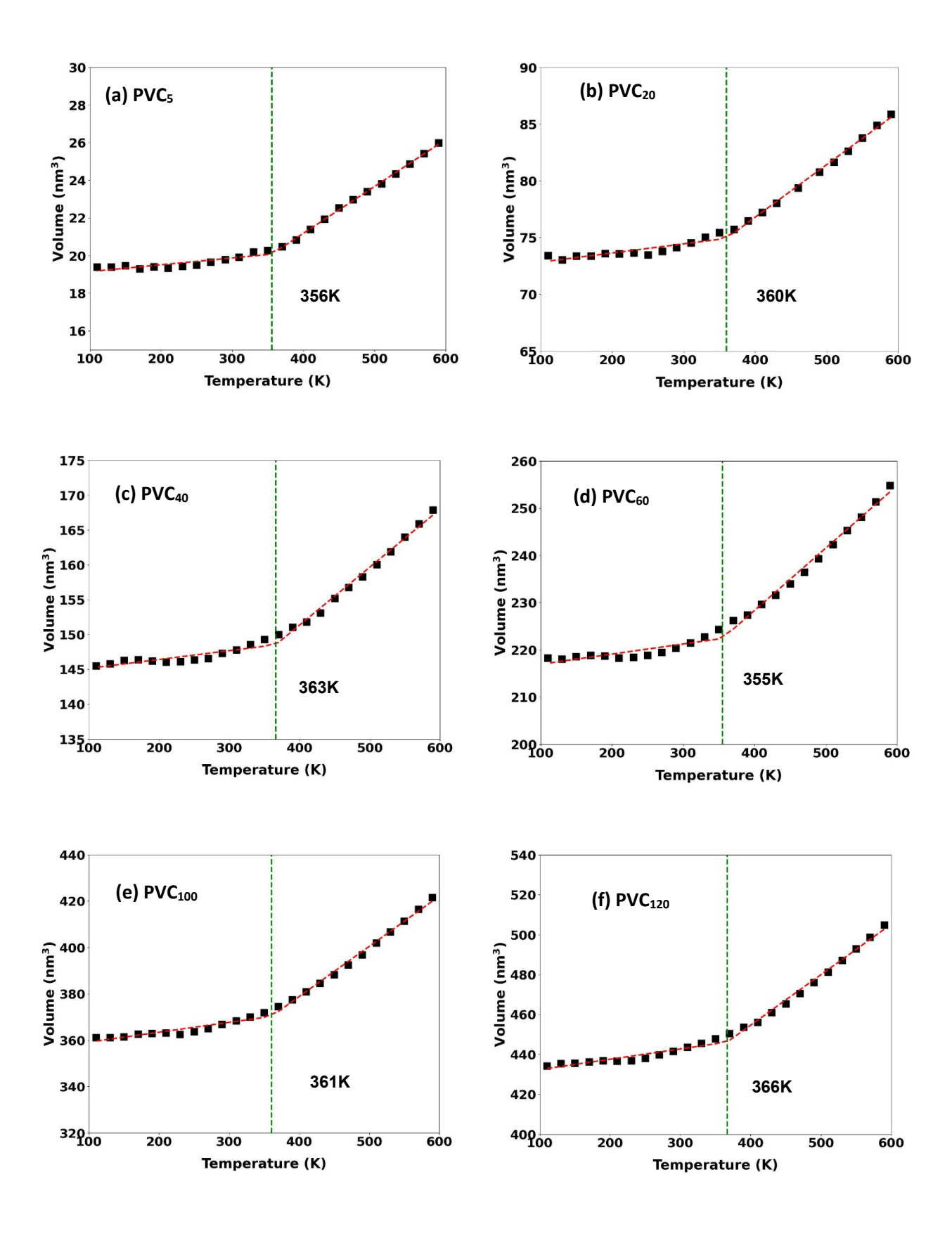
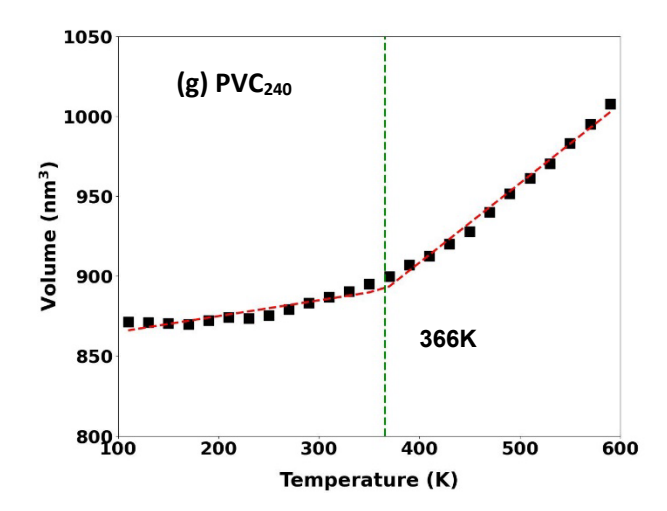


Figure 11. Electrostatic potential of PVC in (a) THF and (b) DMF at 323K

## 3.7 Glass transition temperature

Beyond the previously discussed structural and dynamic characterizations, the calculated  $T_g$  value of the PVC models can offer additional insights into the polymer mechanical behavior. Figure 12 illustrates the trend of  $T_g$  values across various PVC chain lengths, revealing a plateau at approximately 366 K for chains extending 120 units and beyond. This observed behavior suggests that the increased chain length corresponds to an increase in the molecular interactions within the polymer, including entanglement, leading to a higher kinetic energy requirement (temperature) for the transition from the glassy to rubbery state. However, the variations in  $T_g$  values across the different chain lengths remain relatively small, within an 11 K range. Notably, these values are within the experimental  $T_g$  range reported in the literature for PVC [52-55]. While simulated  $T_g$  values generally match experimental ranges (350 K – 370 K), exact values can differ due to varying experimental and simulation conditions.





**Figure 12.** Volume versus temperature plots for PVC melt systems of different chain lengths used to determine  $T_g$  values (indicated on graphs).

### 3.8 Viscosity

To further probe the influence of chain length on the rheological characteristics of PVC, the zero shear viscosity values were determined for each chain length by extrapolating the plot of  $1/\eta$  versus amplitude (see Supporting Information). As depicted in Figure 13, there is a distinct correlation between the melt viscosity and the molecular weight of the polymer. These results are similar with the experimental results of Collins et al. [56], showing a consistent increase in viscosity with increasing chain length. This can be attributed to two predominant factors. First, longer polymer chains present increased drag due to their larger size. Second, there is an enhanced effect of intermolecular attractions as chain length increases. In the molten state, these factors give rise to more entanglements within the polymer matrix. These entanglements pose resistance to shear forces and restrict polymer flow, thereby increasing the viscosity.

To better represent this relationship, the viscosity and polymer molecular weight (M) data are fitted according to Eq. 15:

$$\eta = 7.3M^{0.52} \tag{15}$$

The equation indicates that, while the viscosity does increase with molecular weight, the rate of increase gradually declines for very large chain lengths. This can be rationalized by understanding that beyond a certain threshold of chain length, additional entanglements contribute minimally to the flow properties. In essence, the influence of entanglements on viscosity appears to plateau, marking a limit to the extent they can impede polymer flow.

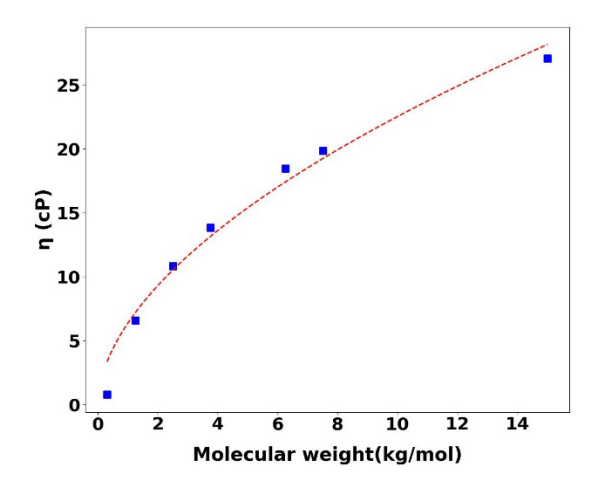


Figure 13. Viscosity versus PVC molecular weight of the melt system at a temperature of 600 K.

#### 4.0 Conclusions

PVC chains of varying lengths (5 – 240 repeat units) have been studied in THF and DMF solvents to understand the influence of the polymer chain length on the polymer structural and dynamic properties in an MD simulation. Most of the polymer properties converge above a chain length of N  $\sim$  120 (PVC<sub>120</sub>). For all chain lengths studied, there exist distinct short-range interactions between the polymer atoms and the solvent atoms. As the PVC chain length increases, the intensity of the first peak in the RDFs decrease and converge with N  $\sim$  120 or more repeat units. Furthermore, the end-to-end distance is found to display a linear relationship with the number of repeat units. The shape descriptors also demonstrate that as the number of repeat units increases, the conformations become less spherically symmetric. The radius of

gyration increases with chain length, indicating that the end-to-end vectors of shorter chains are more correlated than those of longer chains, and thus, the reorientation time is significantly longer. Additionally, the dihedral motions of the polymer backbone become more correlated in longer chains due to constraints imposed by neighboring intermolecular interactions. The surface area per repeat unit and electrostatic potential both tend to converge at N=40 repeat units and above.

While a distribution of chain lengths should be considered when studying real polymer-solvent systems (as well as defects in the polymer backbone), the results of this work suggest that PVC<sub>120</sub> is a reasonable model for capturing the essential physics within a polymer-solvent system. We believe that a PVC model with 100-120 repeat units is able to sufficiently capture the chain entanglement that is representative of much longer chains, consistent with the structures/interactions present in the bulk material. Once the entanglement length is reached, additional repeat units do not significantly affect the polymer's structure and dynamics. This observation also aligns with findings from previous studies [57-59]. Thus, while the molecular weight of an experimental PVC sample is expected to be an order-of-magnitude larger, an atomistic polymer model with approximately 120 repeat units should be sufficient to model its solvation behavior within different prototype solvents. Further studies are warranted to determine the chain-length dependence of other atomistic polymer models on the emergent structural and dynamic properties, to develop a consistent modeling framework for comparing solvation behavior.

### **Declaration of Competing Interest**

The authors declare that they have no known competing financial interests or personal relationships that could have appeared to influence the work reported in this paper.

#### Acknowledgements

This work is supported by the National Science Foundation EFRI E3P (Award #: 2132133). We are grateful to the Alabama Supercomputer Authority for computational support.

# Availability of data and materials.

The datasets generated during and/or analyzed during the current study are available from the corresponding author on reasonable request.

#### References

- 1. Zhao, X., et al., *Plastic waste upcycling toward a circular economy*. Chemical Engineering Journal, 2022. **428**: p. 131928.
- 2. Young, N.P. and N.P. Balsara, *Flory–Huggins Equation*, in *Encyclopedia of Polymeric Nanomaterials*, S. Kobayashi and K. Müllen, Editors. 2021, Springer Berlin Heidelberg: Berlin, Heidelberg. p. 1-7.
- 3. Liu, J.-L. and C.-L. Li, *A generalized Debye-Hückel theory of electrolyte solutions*. AIP Advances, 2019. **9**(1): p. 015214.
- 4. Allison, S.A., J.J. Sines, and A. Wierzbicki, *Solutions of the full Poisson-Boltzmann equation with application to diffusion-controlled reactions*. The Journal of Physical Chemistry, 1989. **93**(15): p. 5819-5823.
- 5. Venkatram, S., et al., Critical Assessment of the Hildebrand and Hansen Solubility Parameters for Polymers. Journal of Chemical Information and Modeling, 2019. **59**(10): p. 4188-4194.
- 6. Akalp, U., et al., *Determination of the Polymer-Solvent Interaction Parameter for PEG Hydrogels in Water: Application of a Self Learning Algorithm.* Polymer (Guildf), 2015. **66**: p. 135-147.
- 7. Hong, P.-D. and H.-T. Huang, *Solvent Effect on Structural Formation and Molecular Mobility of Polyvinyl Chloride Gels*. Polymer Journal, 2000. **32**: p. 789-795.
- 8. Huang, J.-C. and R.D. Deanin, Concentration dependency of interaction parameter between PVC and plasticizers using inverse gas chromatography. Journal of Applied Polymer Science, 2004. **91**(1): p. 146-156.
- 9. Hyde, A.J. and A.G. Tanner, *Light-scattering experiments on polymer-polymer-solvent systems*. Journal of Colloid and Interface Science, 1968. **28**(2): p. 179-186.
- 10. Posharnowa, N., et al., *Polymer–polymer interaction parameters for homopolymers and copolymers from light scattering and phase separation experiments in a common solvent.* The Journal of Chemical Physics, 2001. **115**(20): p. 9536-9546.
- 11. Stillinger, F.H. and T.A. Weber, *Study of melting and freezing in the Gaussian core model by molecular dynamics simulation.* The Journal of Chemical Physics, 1978. **68**(8): p. 3837-3844.
- 12. Noid, D.W., et al., *Computer simulation of the melting process in linear macromolecules*. Macromolecules, 1988. **21**(12): p. 3482-3485.
- 13. Bishop, M., et al., *Investigations of static properties of two-dimensional bulk polymer systems*. The Journal of Chemical Physics, 1981. **75**(11): p. 5538-5542.
- 14. Hentschke, R., B.L. Schürmann, and J.P. Rabe, *Molecular dynamics simulations of ordered alkane chains physisorbed on graphite*. The Journal of Chemical Physics, 1992. **96**(8): p. 6213-6221.

- 15. Bala, V., A Molecular Dynamics Study Of Polymer Chains In Shear Flows and Nanocomposites, in Applied Mathematics. 2022, The University of Western Ontario: Electronic Thesis and Dissertation Repository. 8573.
- 16. Steinhauser, M.O., A molecular dynamics study on universal properties of polymer chains in different solvent qualities. Part I. A review of linear chain properties. The Journal of chemical physics, 2005. **122**(9): p. 094901.
- 17. Lin, E.Y., et al., Effect of surface properties and polymer chain length on polymer adsorption in solution. The Journal of Chemical Physics, 2021. **155**(3): p. 034701.
- 18. Harmandaris, V.A., V.G. Mavrantzas, and D.N. Theodorou, *Atomistic Molecular Dynamics Simulation of Polydisperse Linear Polyethylene Melts*. Macromolecules, 1998. **31**(22): p. 7934-7943.
- 19. Lee, S., C.W. Frank, and D.Y. Yoon, *Interface Characteristics of Neat Melts and Binary Mixtures of Polyethylenes from Atomistic Molecular Dynamics Simulations*. Polymers, 2020. **12**(5): p. 1059.
- 20. Mavrantzas, V.G., Using Monte Carlo to Simulate Complex Polymer Systems: Recent Progress and Outlook. Frontiers in Physics, 2021. 9: p. 661367.
- 21. Nicholls, I.A., et al., *The Use of Computational Methods for the Development of Molecularly Imprinted Polymers*. Polymers, 2021. **13**(17): p. 2841.
- 22. Paquet, E. and H.L. Viktor, *Computational Methods for Ab Initio Molecular Dynamics*. Advances in Chemistry, 2018. **2018**: p. 9839641.
- 23. Singh, V., et al., Recent trends in computational tools and data-driven modeling for advanced materials.

  Materials Advances, 2022. **3**(10): p. 4069-4087.
- 24. Arbe, A., F. Alvarez, and J. Colmenero, *Insight into the Structure and Dynamics of Polymers by Neutron Scattering Combined with Atomistic Molecular Dynamics Simulations*. Polymers, 2020. **12**(12): p. 3067.
- 25. Oster, K., et al., *Dehydrochlorination of PVC in multi-layered blisterpacks using ionic liquids*. Green Chemistry, 2020. **22**(15): p. 5132-5142.
- 26. Lewandowski, K. and K. Skórczewska, *A Brief Review of Poly(Vinyl Chloride) (PVC) Recycling*. Polymers (Basel), 2022. **14**(15): p. 3035.
- 27. Zhou, X.-L., et al., *Upcycling waste polyvinyl chloride: One-pot synthesis of valuable carbon materials and pipeline-quality syngas via pyrolysis in a closed reactor.* Journal of Hazardous Materials, 2022. **427**: p. 128210.
- 28. Neelov, I., S. Niemelä, and F. Sundholm, *A computer simulation of the molecular properties of amorphous poly(vinyl chloride)*, *PVC*. Journal of Non-Crystalline Solids, 1998. **235-237**: p. 340-345.
- 29. Li, M., et al., Polyvinyl Chloride Nanoparticles Affect Cell Membrane Integrity by Disturbing the Properties of the Multicomponent Lipid Bilayer in Arabidopsis thaliana. Molecules, 2022. 27(18): p. 5906.

- 30. Kempfer, K., et al., Development of Coarse-Grained Models for Polymers by Trajectory Matching. ACS Omega, 2019. 4(3): p. 5955-5967.
- 31. Wu, C., Coarse-grained molecular dynamics simulations of stereoregular poly(methyl methacrylate)/poly(vinyl chloride) blends. Journal of Polymer Science Part B: Polymer Physics, 2015. 53(3): p. 203-212.
- 32. Nguyen, D., L. Tao, and Y. Li, *Integration of Machine Learning and Coarse-Grained Molecular Simulations for Polymer Materials: Physical Understandings and Molecular Design.* Frontiers in Chemistry, 2022. 9: p. 1280.
- 33. Patra, T.K. and J.K. Singh, *Polymer directed aggregation and dispersion of anisotropic nanoparticles*. Soft Matter, 2014. **10**(11): p. 1823-1830.
- 34. Abraham, M.J., et al., *GROMACS: High performance molecular simulations through multi-level parallelism from laptops to supercomputers.* SoftwareX, 2015. **1-2**: p. 19-25.
- 35. Kutzner, C., et al., *GROMACS in the Cloud: A Global Supercomputer to Speed Up Alchemical Drug Design.* J Chem Inf Model, 2022. **62**(7): p. 1691-1711.
- 36. Humphrey, W., A. Dalke, and K. Schulten, *VMD: visual molecular dynamics*. J Mol Graph, 1996. **14**(1): p. 33-8, 27-8.
- 37. Jorgensen, W.L., D.S. Maxwell, and J. Tirado-Rives, *Development and Testing of the OPLS All-Atom Force Field on Conformational Energetics and Properties of Organic Liquids*. Journal of the American Chemical Society, 1996. **118**(45): p. 11225-11236.
- 38. YABE, M., et al., Development of PolyParGen software to facilitate the determination of molecular dynamics simulation parameters for polymers. Journal of Computer Chemistry, Japan-International Edition, 2019. 5: p. 2018-0034.
- 39. Dodda, L.S., et al., LigParGen web server: an automatic OPLS-AA parameter generator for organic ligands. Nucleic Acids Res, 2017. **45**(W1): p. W331-w336.
- 40. Dodda, L.S., et al., 1.14\*CM1A-LBCC: Localized Bond-Charge Corrected CM1A Charges for Condensed-Phase Simulations. The Journal of Physical Chemistry B, 2017. **121**(15): p. 3864-3870.
- 41. Martínez, L., et al., *PACKMOL: A package for building initial configurations for molecular dynamics simulations*. Journal of Computational Chemistry, 2009. **30**(13): p. 2157-2164.
- 42. Bussi, G., D. Donadio, and M. Parrinello, *Canonical sampling through velocity rescaling*. The Journal of Chemical Physics, 2007. **126**(1): p. 014101.
- 43. Nosé, S. and M.L. Klein, *Constant pressure molecular dynamics for molecular systems*. Molecular Physics, 1983. **50**(5): p. 1055-1076.
- 44. Darden, T., D. York, and L. Pedersen, *Particle mesh Ewald: An N·log(N) method for Ewald sums in large systems*. The Journal of Chemical Physics, 1993. **98**(12): p. 10089-10092.

- 45. Hess, B., et al., *LINCS: A linear constraint solver for molecular simulations*. Journal of Computational Chemistry, 1997. **18**(12): p. 1463-1472.
- 46. Brehm, M., et al., *TRAVIS—A free analyzer for trajectories from molecular simulation*. The Journal of Chemical Physics, 2020. **152**(16): p. 164105.
- 47. Shakarji, C.M., *Least-squares fitting algorithms of the NIST algorithm testing system.* Journal of research of the National Institute of Standards and Technology, 1998. **103**(6): p. 633.
- 48. Santos, M.S., F.W. Tavares, and E.C. Biscaia Jr, *MOLECULAR THERMODYNAMICS OF MICELLIZATION: MICELLE SIZE DISTRIBUTIONS AND GEOMETRY TRANSITIONS.* Brazilian Journal of Chemical Engineering, 2016. **33**.
- 49. Hess, B., Determining the shear viscosity of model liquids from molecular dynamics simulations. The Journal of chemical physics, 2002. **116**(1): p. 209-217.
- 50. Bhattacharjee, S.M., A. Giacometti, and A. Maritan, *Flory theory for polymers*. Journal of Physics: Condensed Matter, 2013. **25**(50): p. 503101.
- 51. Ricci, E., et al., Molecular Simulations and Mechanistic Analysis of the Effect of CO 2 Sorption on Thermodynamics, Structure, and Local Dynamics of Molten Atactic Polystyrene. Macromolecules, 2020. 53: p. 3669-3689.
- 52. Lindström, A. and M. Hakkarainen, Environmentally friendly plasticizers for poly (vinyl chloride)—
  Improved mechanical properties and compatibility by using branched poly (butylene adipate) as a polymeric plasticizer. Journal of applied polymer science, 2006. 100(3): p. 2180-2188.
- 53. Rohling, J., et al., *Thermal lens versus DSC measurements for glass transition analysis of polymer*. Analytical Sciences/Supplements, 2002. **17**(0): p. s103-s105.
- 54. Ziska, J., J. Barlow, and D. Paul, *Miscibility in PVC-polyester blends*. Polymer, 1981. **22**(7): p. 918-923.
- Da Silva, M.A., et al., Polyvinylchloride (PVC) and natural rubber films plasticized with a natural polymeric plasticizer obtained through polyesterification of rice fatty acid. Polymer Testing, 2011. **30**(5): p. 478-484.
- 56. Collins, E.A. and C.A. Daniels, *PVC melt rheology III: The effect of order and molecular weight on the shear rate dependence.* Polymer Engineering & Science, 1974. **14**(5): p. 357-361.
- 57. Deady, M., et al., Evaluation of the kinetic parameters for styrene polymerization and their chain length dependence by kinetic simulation and pulsed laser photolysis. Die Makromolekulare Chemie, 1993. **194**(6): p. 1691-1705.
- 58. Gao, Y., et al., *Influence of various nanoparticle shapes on the interfacial chain mobility: a molecular dynamics simulation.* Physical Chemistry Chemical Physics, 2014. **16**(39): p. 21372-21382.

59. Wu, Y.-H., D.-M. Wang, and J.-Y. Lai, Effects of Polymer Chain Length and Stiffness on Phase Separation Dynamics of Semidilute Polymer Solution. The Journal of Physical Chemistry B, 2008. **112**(15): p. 4604-4612.